AUT Journal of Electrical Engineering
10.22060/EEJ.2026.25097.5837

Design of a Hexagonal Stepped Impedance Resonator Textile Antenna for Robust Biomedical and Environmental Monitoring

Yeddu Eswar Vasanth Kumar[1,*], Gurindapalli Rajita[2] and Kokilagadda Phaninder Vinay[3]

[1] M.Tech, (Ph.D), GIET University, Gunupur, Odisha, India
[2] Ph.D, Dr. G. Rajita, GIET University, Gunupur, Odisha, India
[1, 3] Ph.D, Dr. K. P. Vinay, RAGHU Engineering College, Vskp, A.P, India

[*]Corresponding author: email address: y.eswaravasanth@giet.edu

ABSTRACT: This work presents a compact, hexagon-shaped wideband antenna designed for wearable applications in the Industrial, Scientific, and Medical band. The antenna is fabricated on a flexible felt substrate with a dielectric constant of 1.22 and a loss tangent of 0.016, achieving a compact footprint of 35 × 30 × 2 mm³. A Coplanar Waveguide feed integrated with a Stepped Impedance Resonator is employed to enhance impedance matching and bandwidth performance. The felt substrate exhibits excellent mechanical durability and electromagnetic stability under repeated bending and typical wear conditions, ensuring reliable long-term operation. The proposed antenna achieves a peak gain of 7.31 dB at 5.82 GHz and maintains a Specific Absorption Rate of 1.08 W/kg for 1 g of tissue, which is well within regulatory safety limits. Beyond communication, the antenna demonstrates moisture-sensing capability, exhibiting a consistent downward shift in resonant frequency with increasing substrate humidity. While stable under bending, excessive moisture leads to detuning and impedance mismatch. The strong correlation between simulated and measured results validates the proposed design as a robust and multifunctional solution for wearable biomedical and ultra-wideband sensing applications.

Keywords: CPW, ISM, SIR, Textile Fabric, Wearable Medical Device

1. INTRODUCTION

In recent years, Wireless Body Area Networks (WBANs) have enabled remarkable advancements in wireless systems, supporting a wide range of applications such as wearable devices, emergency response systems, and patient monitoring. For these on-body applications, antennas must be durable, lightweight, and comfortable when integrated into clothing. However, a significant challenge arises from performance degradation due to near-field coupling when the antenna is placed close to the skin. To address this issue, compact planar monopole antennas are being designed specifically for wearable WBAN applications, frequently incorporating periodic structures such as metamaterials and antenna arrays to improve overall performance. The Microstrip Antenna Reflector is intended for biomedical applications requiring an electromagnetic band gap (EBG) [1]. A unique, small, broadband, and simple PIFA constructed utilizing conductive fabrics, suitable for wireless body area network applications, is described. Slotted PIFAs outperform non-slotted ones with similar materials and radiative properties [2]. The antenna being used is tiny and wearable, operating in the 2.36-2.4 GHz medical body-area network spectrum. To allow the antenna, a truncated Meta surface of two by two I-shaped components is placed beneath a planar monopole [3]. This study presents a flexible antenna based on CSRR that may be used for medical and telemetry applications operating in the 2.4-GHz industrial, scientific, and medical (ISM) radio band. The antenna is made of denim (jeans) to create a low profile, flexibility, and reduced bulk. To increase flexibility and decrease loss from coaxial feed, a CPW feed is utilized. The goal of the flexible CSRR antenna's design is to achieve maximum gain while minimizing losses [4]. This research presents artificial magnetic conductor structure with folded dipole antenna for covid -19 patients, surgical mask placed on the human mouth [5]. The antenna exhibits enhanced impedance bandwidth. It is suggested to use graphene as the conducting material and Kapton polyimide as the substrate for a flexible dual-band antenna supplied by a coplanar waveguide (CPW)[6]. This study investigates on a metallic loop antenna with coplanar feed line fabricated using cotton fabric with artificial magnetic conductor [7]. This work proposes a small, conformal, all-textile wearable antenna for the 2.45 GHz Industrial, Scientific, and Medical (ISM) band. The integrated design has a monopole radiator and a 2 × 1 Electromagnetic Band Gap (EBG) array, resulting in a tiny form factor ideal for wristband applications. An EBG unit cell is optimized to function in the appropriate operating band, and the findings are then used to maximize bandwidth using floating EBG ground [8]. This communication offers a flexible wearable antenna that is low-profile and wideband, designed to function at the 2.45 GHz WBAN band. A CPW-fed monopole antenna supported by an artificial magnetic conductor (AMC) to serve as a reflector makes up the recommended antenna. R03003 is the dielectric substrate used in the most recent AMC-integrated architecture. The 3.5 GHz Wi MAX spectrum is covered by the addition of wideband AMC with a monopole antenna, which increases bandwidth [9]. The design and analysis of miniature implantable conformal patch antennas for use in biomedical applications are presented in this study. To accomplish conformability, a polyimide substrate material is taken into consideration. With a monopole structure and split ring resonator operated at 2.41GHz using implanted coplanar waveguide [10]. In order to increase gain, bandwidth, and efficiency, a Coplanar Waveguide (CPW) fed antenna including a

T-type slot and Partially Reflecting Surface (PRS) is introduced. The antenna has been downsized to achieve a 46.50% decrease in size. The C band is covered by the little antenna [11]. By loading a stepped-impedance resonator (SIR), a unique miniaturized band pass filter is proposed in this study. Due to SIR's inherent properties, a third-order bandpass filter with SIR is introduced, which reduces size by 38% when compared to the traditional hairpin-line filter. The use of two complementary split-ring resonators (CSRR) DGSs allows for additional miniaturization due to the electrical tape gap effect of a DGS [12]. The growing trends of wearable and flexible wireless communication systems can be attributed to their smart applications for continuous living, particularly in wellbeing observe. Although tough and lightweight, flexible antennas struggle to withstand mechanical stress. Their light weight, cost-effectiveness, ease of manufacture, and the availability of affordable flexible substrates are making flexible electronic systems exciting area for consumer electronics of the future. Bendable antennas can be categorized into four main types: substrate integrated waveguide antennas, membrane-based antennas, wearable textile antennas, and flexible 3D printed antennas. Additionally, four more types of flexible antennas are categorized based on the substrate, including carbon nanotube antennas, textile antennas, micro fluidic antennas, and polymer-based antennas. Polymer-based antennas rely on materials that resonate at millimeter wave frequencies for their substrates [19-21]. An irregular octagonal two-port textile MIMO antenna on a 40×50 mm jeans substrate (εeff = 1.6, h = 1 mm) covers 4.35–7.0 GHz with 6.74 dB gain and 28.5 dB isolation, suitable for N79, Wi-Fi 5/6, V2X, and DSRC bands [32]. A dual-wideband denim-textile monopole antenna for wearable use operates over 2.2–4.0 GHz and 5.3–10.0 GHz, with substrate properties verified by DAC and ring-resonator methods. It exhibits stable performance under bending, and SAR in head and abdomen models remains within safe limits [33]. A wideband textile coplanar Vivaldi antenna using a 1 mm felt substrate and copper tape achieves 2.6–8.7 GHz bandwidth ($|S11| \approx -44.9$ dB at 3 GHz, ~107% FBW). Integrated with IoT sensors, it enables reliable temperature and SpO_2 data transmission for wearable applications. [34]. The lightweight planar textile antenna offers omnidirectional radiation with vertical polarization, covering Wi-Fi 2.4/5/6 GHz bands (2.4–2.5 GHz, 4.6–7.2 GHz BW). For 500 mW input and a 2 mm air gap, the peak SAR is 1.053 W/kg, and the antenna size is π (50 mm)² × 6 mm. [35]. The antenna with modified elliptical patches, L-shaped stubs, and a circular decoupling ring achieves >25 dB isolation, 310/950 MHz bandwidth, and 8.3/13.0 dBi gain at 3.5/5.2 GHz. It performs consistently in pocket placements, with very low ECC (0.006/0.002) and SAR within FCC/ICNIRP limits [36]. A compact U-shaped circularly polarized textile antenna on a single-layer denim substrate resonates at 2.45 GHz, offering ~55% ARBW, ~64% IBW, and ~5.1 dBi gain. It shows stable performance under bending and on-body use, covering LTE, MBAN, WPAN, and WLAN bands [37]. A compact multiband denim-textile monopole antenna for patient tracking covers NB- IoT (1.8 GHz), RFID/ISM (2.45/5.8 GHz) with 310/960/1140 MHz bandwidth and 3.7/5.3/9.6 dBi gain. It ensures up to 100 m range, SAR within limits, and durable, comfortable integration into clothing [38]. The polymer's low permittivity inherently enhances bandwidth, while its softness simplifies antenna fabrication. Notably, certain polymers introduce unique properties, such as flexibility and photo sensitivity that ceramics do not offer. The textile antenna represents one of the most

innovative and advanced areas of research. Wearable antennas should be discreet and unobtrusive when attached to the human body like clothing. Textile antennas utilize non-conductive substrates like felt, nylon, Dacron, denim, and others. Since textile materials typically have a low dielectric constant, the relative permittivity becomes a vital factor in antenna design. The antenna will have better bandwidth and impedance due to a reduction in surface wave losses.

This research introduces an innovative compact hexagonal textile antenna designed specifically for wearable ISM band applications, addressing several challenges in wearable wireless communication and sensing technologies. By utilizing a flexible felt substrate with exceptional durability and stable dielectric properties, coupled with a Coplanar Waveguide (CPW) feed integrated with a Stepped Impedance Resonator (SIR), this work overcomes common issues related to antenna flexibility, mechanical stress, and environmental sensitivity. The design ensures reliable performance even under repeated bending and typical wear conditions, which are critical for long-term wearable operation. Moreover, the antenna's dual functionality as both a communication device and a moisture sensor represents a significant advancement in multifunctional wearable electronics. The moisture-dependent resonance shift enables passive environmental and physiological sensing without extra components, lowering system complexity and power use. Comprehensive SAR analysis and moisture-detuning evaluation confirm safe, resilient performance, advancing multifunctional wearable and UWB antenna technologies.

2. ANTENNA DESIGN

This analysis introduces a hexagonal coplanar waveguide fed antenna with step impedance resonator technology on a felt substrate (ε_r = 1.22, $tan\ \delta$ = 0.016) for wearable ISM-band operation at 5.82 GHz. The compact 35 × 30 × 2 mm³ design suits WBAN integration, leveraging felt's superior electrical properties detailed in Table 1.

Table 1.Flexible substrate dielectric constants

Dielectric material	Dielectric Constant Value
Denim	1.70
Silk	1.750
Felt	1.220
Cotton	1.60
Fleece	1.170

The antenna is built on a coplanar waveguide framework utilizing specific design dimensions shown in Table 2. The characteristic impedance can be determined from the microstrip feed line width W_f = 2 mm and the gap g = 3 mm based on Equations (1) to (3). The calculated characteristic impedance is 51.02 Ω, closely matching the standard 50 Ω system impedance [11].

$$Z_0 = \frac{Z_{air}}{\varepsilon_e} \quad (1)$$

Where

$$Z_{air} = 60\ln\left[\frac{F_1 h}{w} + \sqrt{1 + \left(\frac{2h}{w}\right)^{\wedge 2}}\right] \quad (2)$$

$$\varepsilon_e = \sqrt{\frac{\varepsilon_r + 1}{2}} \text{ for } w/h << 1 \quad (3)$$

Where Z_0 is the characteristics impedance, Z_{air} impedance of free space, ε_e is effective permittivity, ε_r relative permittivity W/h is ratio of width and height of substrate, F is frequency of radiating patch.

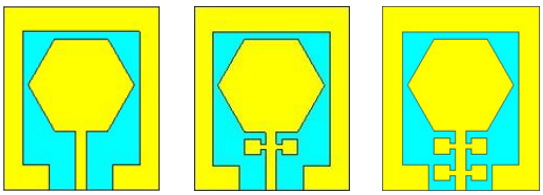

Fig. 1.Evolution of design

Figure 1 illustrates the stepwise evolution of the wearable ISM-band patch antenna, highlighting how the successive integration of stepped-impedance resonator (SIR) sections refines its resonant behavior. The design process begins with a basic hexagonal patch and microstrip feed, which establishes a fundamental resonance but offers, limited frequency control. To address this, a single SIR is introduced between the feed and the patch; its alternating high- and low-impedance sections effectively increase the antenna's electrical length without changing its physical size, thereby shifting the resonance into the target ISM band and improving the impedance match. Finally, a second, cascaded SIR is integrated to provide finer tuning flexibility, sharper suppression of spurious modes, and enhanced bandwidth control. This final dual-SIR configuration enables the precise frequency alignment and enhanced performance that make the antenna well-suited for demanding wearable ISM applications.

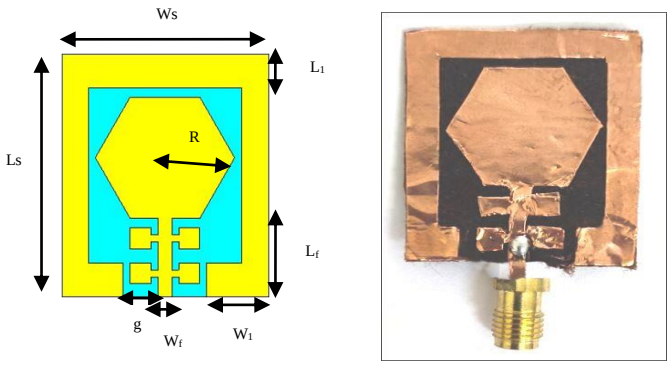

(a) (b)

Fig. 2 .(a) Simulated View (b) Fabricated View of final design

Table 2 .Antenna dimensions

Parameter	Dimensions (mm)	Parameter	Dimensions (mm)
Ws	30	L_f	15
Ls	35	L_1	5
R	10	W_1	11
W_f	2	G	3

All units are in millimeter (mm)

Felt was chosen as the substrate material because it offers an optimal balance of electrical performance and mechanical properties compared to other textiles, such as flexibility, light weight, and durability. The foundational design of the antenna, illustrated in Figure 2, was developed and simulated in CST Microwave Studio to validate the proposed geometry, feeding technique, and ground plane configuration. This initial simulation campaign was crucial for establishing the baseline resonant frequency, impedance match, and radiation characteristics of the antenna before proceeding with physical prototyping and optimization. [18, 23, 25]. The standard resonance frequency of an RLC circuit is:

$$f_r = \frac{1}{2\Pi\sqrt{LC}} \tag{4}$$

f_r is the resonating frequency, L is inductance, C is the capacitance

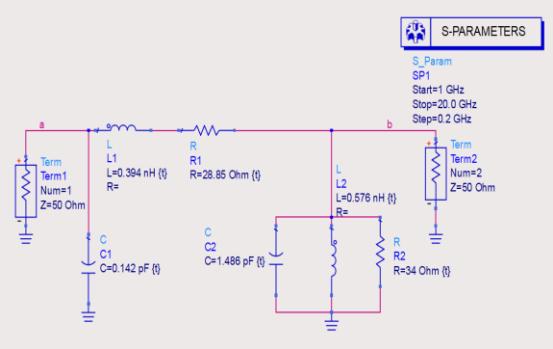

Fig. 3 .Equivalent Circuit of proposed design

The electrical behavior of the proposed antenna can be modeled by the equivalent RLC resonant circuit shown in Equation 4. In this model, the antenna's performance is approximated by a circuit consisting of a resistor (R), an inductor (L), and a capacitor (C). At the resonant frequency, the inductive and capacitive reactance cancels each other out, which results in purely resistive impedance. This condition allows for minimum impedance and maximum current flow, signifying efficient energy transfer. Figure 3 illustrates this equivalent circuit, which was designed and simulated in Advanced Design System (ADS). By tuning the RLC parameters within the software, the S-parameter response was analyzed, confirming that the circuit successfully models the antenna's resonance at 5.82 GHz.

Fig. 4 .Reflection coefficient value of proposed antenna using ADS tool

The antenna's resonant frequency and bandwidth were precisely controlled by tuning the physical dimensions of the stepped-impedance resonator (SIR) sections, which correspond to the inductance (L), capacitance (C), and resistance (R) values in the equivalent circuit model shown in Figure 4. By enhancing the impedance contrast between the SIR sections or by cascading a second SIR, the design achieved a sharper pass band and improved impedance matching. The corresponding physical dimensions were then optimized in CST Microwave Studio to replicate this desired S_{11} response within the final hexagonal patch configuration.

3. RESONATOR DESIGN

This analysis underscores the critical role of the Stepped Impedance Resonator (SIR) filter in defining the patch antenna's final performance, as illustrated by the resonance profile transformation in Figure 5. By carefully optimizing the impedance ratio and electrical lengths of the alternating high- and low-impedance transmission line sections, the dual SIR functions as an integrated bandpass filter. This structure provides precise frequency control, significantly improves the impedance match, and creates inherent bandpass filtering. The reflection coefficient results, shown in Figure 7, validate the success of this approach, confirming that the antenna system is efficiently tuned to the 5.82 GHz ISM frequency. This combined filter-antenna architecture is therefore highly suitable for compact, wearable applications that require both a selective frequency response and robust performance [12].

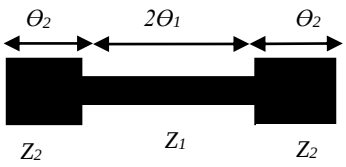

Fig. 5 .Stepped impedance resonator

The condition of resonance for SIR signal is given by

$$\frac{Z_2}{Z_1} = tan\theta_1 \, tan\theta_2 = K \tag{5}$$

Where, Z_1 is the characteristic impedance of the narrow (high-impedance) section, Z_2 is the characteristic impedance of the broad (low-impedance) section, θ_1 is the electrical length of the narrow section, θ_2 is the electrical length of the broad section, K is impedance ratio and θ_T is the overall electrical length of the transmission line.

$$\theta_T = \theta_1 + \theta_2 \tag{6}$$

θ_T is minimum when

$$\theta_1 = \theta_2 = tan^{-1}\sqrt{K} \tag{7}$$

for 0 <K < 1, we get the minimum line length of the resonator.

Table 3 .Filter Dimensions

Parameter	Dimensions (mm)
L1,L2	3, 1
W1,W2	2, 0.5

All units are in millimeter (mm)

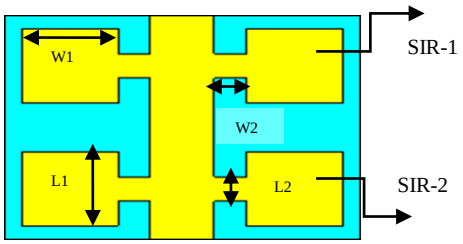

Fig. 6 .Schematic view of dual SIR filter

Table 3 describes *L1* and *W1* as the broad, low impedance sections, whereas *L2* and *W2* define the narrow, high impedance sections based on Equations 5 to 7. These dimensions set Z_1 and Z_2, thereby determining the impedance ratio $K=Z_2/Z_1$ and the filter's selectivity shown in Figure 6. Selecting appropriate lengths and widths tunes the electrical lengths $\theta_1$and θ_2, which fix the resonant frequency. Balanced section lengths yield a compact SIR that can be tuned to 5.8 GHz, shifting the patch's natural resonance to the target band while imparting intrinsic bandpass behavior shown in Figure 7. Thus, coordinated control of impedances and electrical lengths provides an efficient, space saving means of frequency tuning and bandwidth management for wearable ISM patch antennas [22-24].

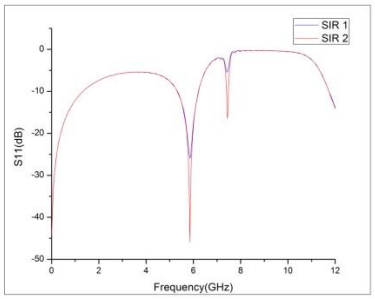

Fig. 7 .Reflection coefficient analysis of SIR filters tuned at 5.8GHz

4. RESULTS

The antenna was developed for the 5.8 GHz ISM band using a sequential design process. The initial step involved establishing the coplanar waveguide (CPW) feed and primary radiator. Subsequently, a stepped impedance resonator (SIR) was integrated to tune the antenna to its target operating frequency. Both simulated and measured S11 and VSWR parameters, obtained with a Rohde & Schwarz ZVL network analyzer, demonstrate strong agreement. Minor discrepancies observed between the results are attributed to fabrication tolerances from the copper tape adhesive process and variations in SMA connector coupling losses. Overall, the SIR-fed configuration successfully tunes the patch antenna to 5.8 GHz while providing an inherent bandpass filtering characteristic.

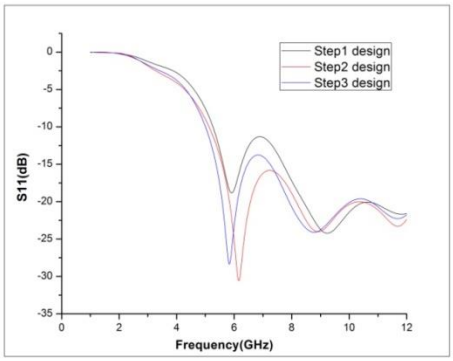

Fig. 8 .Reflection coefficient analysis of proposed design in steps

Figure 8 illustrates the return loss at each design stage of the antenna, emphasizing the gradual evolution of its frequency response. As the coplanar structure is incrementally incorporated from Step 1 to Step 3, as shown in Figure 1, the resonant frequency progressively shifts downward. The final return loss response, presented in Figure 8, confirms that the optimized Step-3 configuration resonates at 5.82 GHz and offers an ultra- wideband operating bandwidth.

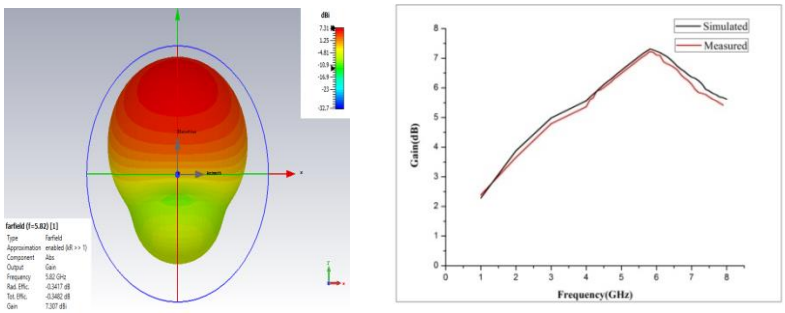

(a) (b)

Fig. 9 .Proposed design (a) 3D gain plot (b) Gain vs Frequency

Figure 9(a) shows the 3D far-field radiation pattern at 5.82 GHz, indicating a peak gain of 7.31 dB with the main lobe directed along the antenna's bore sight. A comparison of the simulated and measured gain responses is presented in Figure 9(b), demonstrating strong agreement. The simulated peak gain of 7.31 dB at 5.82 GHz corresponds closely with the

measured peak gain of 7.22 dB. This minor 0.09 dB deviation is attributed to practical factors such as connector losses and fabrication tolerances. Across the 5.6–6.0 GHz range, the realized gain remains above 6.8 dB, and the radiation efficiency is estimated to be between 82% and 86%. Furthermore, the antenna achieves a front-to-back ratio exceeding 14 dB at its resonant frequency, which confirms the effectiveness of the ground plane and CPW design.

(a) (b)

Fig. 10 .Vector network analyzer measurements of the proposed antenna: (a) S11 and (b) VSWR

Figure 10 illustrates the S11 measurement setup employing a vector network analyzer to characterize the proposed antenna's performance. The –10 dB return-loss criterion, equivalent to a VSWR of ~1.92:1, ensures ~90% power transfer with minimal reflection due to impedance matching. Measured S11 and VSWR traces across the operating band experimentally validate excellent matching and efficient radiation.

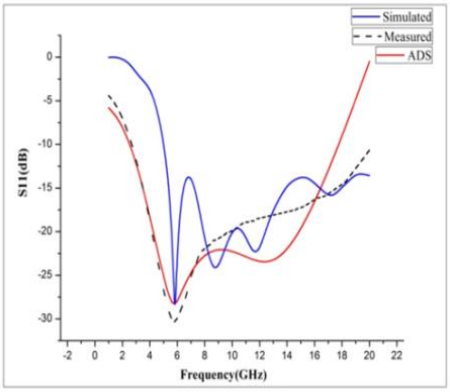

Fig. 11 .Reflection Coefficient analysis using CST, ADS and VNA

Figure 11 compares the simulated return loss from CST and ADS with the measured response using a vector network analyzer, demonstrating excellent agreement across all curves. A pronounced resonance appears at 5.8 GHz, with the measured S11 deviating by less than 0.5 dB from simulations at the minimum. This close correlation validates the design model's accuracy and the efficacy of the impedance-matching approach.

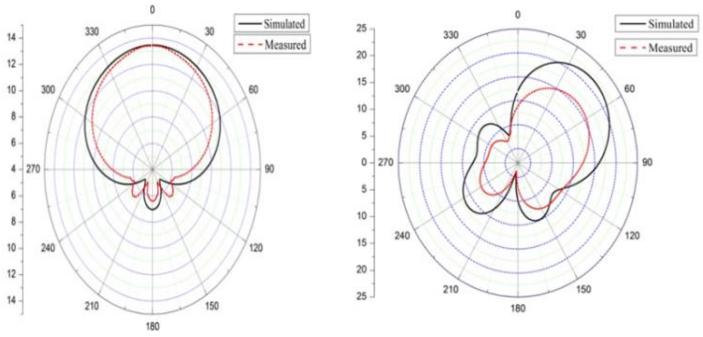

(a) (b)

Fig.12 .(a) E- field radiation pattern (E- plane) at 0° and (b) H- field radiation pattern (H- plane) at 90°

Figure 12 shows the far- field radiation patterns at 5.8 GHz in the principal E- plane (ϕ=0°) and H- plane (ϕ=90°). The E- plane cut exhibits a broadside dominant lobe with side lobes below −15 dB, while the H- plane cut remains stable with quasi omnidirectional characteristics suitable for on- body links. Simulated and measured patterns agree closely, with HPBWs of ~68° (E- plane) and ~72° (H- plane), confirming robust radiation behavior at the design frequency.

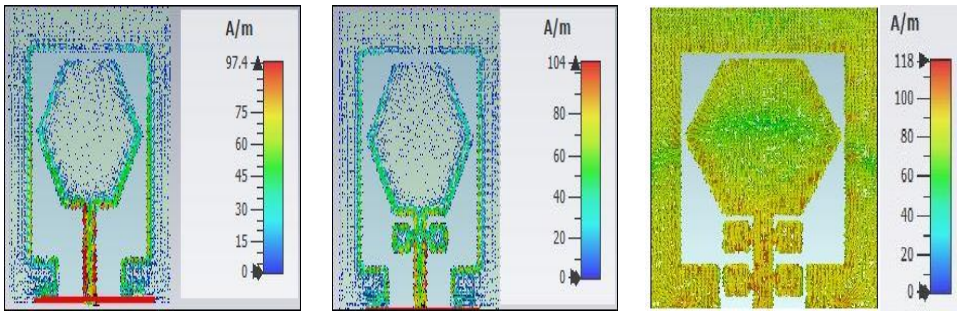

Step 1 Step 2 Step 3

Fig. 13 .Surface current distribution from Step 1 to Step 3

Figure 13 summarizes the progressive modification of the surface- current distribution across the three design steps. In Step 1, the current is mainly concentrated on the CPW feed and the lower region of the hexagonal radiator, indicating a fundamental monopole type excitation. With the introduction of the stepped impedance resonator(s) in Steps 2 and 3, the current becomes increasingly confined to the resonator sections and the feed patch junction, evidencing stronger coupling and an increased effective electrical length. Consequently, the final (dual SIR) configuration improves input impedance matching and yields a more band selective response centered around 5.8 GHz while preserving dominant radiation from the main radiator. [28-30].

4.1 Bending Analysis

To assess its feasibility for on-body applications, the flexible antenna's performance was examined under mechanical bending conditions. The antenna was conformed along the XOZ-plane with bending radii of 40 mm, 50 mm, and 60 mm to replicate the typical curvatures of the human chest and limbs.

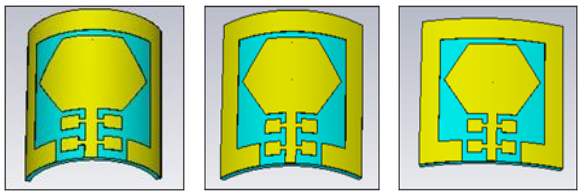

40mm 50mm 60mm

Fig. 14 .Proposed design antenna under XOZ-plane bending condition

As illustrated in Figure 14, the simulated results reveal that the reflection coefficient remains largely consistent across all bending scenarios. This stability confirms robust impedance matching and minimal frequency detuning, demonstrating that the antenna maintains its 5.8 GHz resonance effectively when transitioning from a flat to a bent configuration.

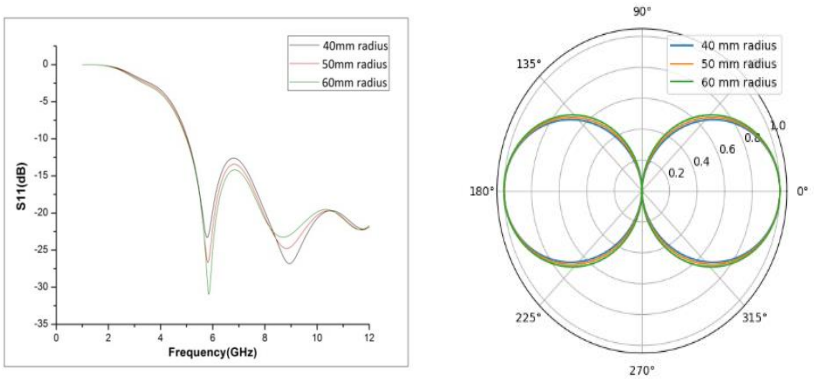

(a) (b)

Fig. 15 .Proposed antenna under different bending radii (a) S11 versus frequency (b) Radiation patterns

Under bending, the antenna maintains a clear 5.8 GHz resonance for radii of 40–60 mm, with all cases achieving $|S11| < -10$ dB, confirming acceptable impedance matching for ISM band wearable operation. The negligible resonance shift indicates that curvature only weakly perturbs the effective electrical length and input impedance, evidencing good mechanical–electromagnetic robustness. Although the minimum |S11| slightly degrades with increasing radius, the operational bandwidth and the alignment of higher order resonances are preserved. The corresponding radiation patterns for the three radii largely overlap, with only minor variations near the main lobes, while the main lobe directions and null locations remain essentially unchanged, confirming pattern integrity under bending.

4.2 **Specific Absorption Rate**

The Specific Absorption Rate (SAR) is the standard metric used to quantify the amount of radio frequency (RF) energy absorbed per unit mass of biological tissue. It is a critical measure for ensuring the safety of wearable and mobile devices. The SAR value can be calculated from the electric field within the tissue using the following formula [25].

$$SAR = \frac{\sigma E^{\wedge 2}}{\rho} \tag{8}$$

In the above equation, E indicates electric field strength, ρ is mass density and. σ denotes conductivity.

Table 4 .Human Tissue Characteristics and Properties

Tissue	Dielectric permittivity *(εr)*	Conductivity *(σ)*	Density (Kg/m^3)	Thickness (mm)
Skin	37.95	1.490	1001	2
Fat	5.27	0.110	900	5
Muscle	52.67	1.770	1006	13

All units are in millimeter (mm)

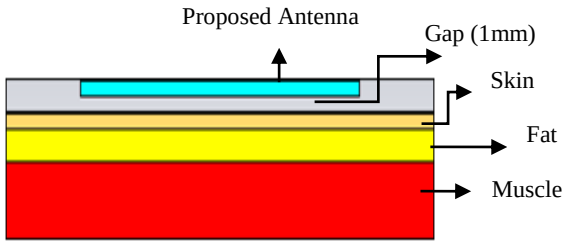

Fig. 16 Simulated human tissue model

Figure 16 depicts a multilayer human tissue phantom (skin: 2 mm, fat: 5 mm, muscle: 13 mm) constructed per Table 4 to evaluate on-body performance, with the antenna separated by a 1 mm air gap. For a 35 × 30 mm² cross-section, tissue masses are 2.10 g (skin, 1001 kg/m³), 4.73 g (fat, 900 kg/m³), and 13.73 g (muscle, 1006 kg/m³). This standoff minimizes near-field coupling losses, detuning, bandwidth narrowing, efficiency reduction, and SAR elevation relative to 0–2 mm gaps, where here |S11| degrades 5–10 dB and resonance shifts 3–10% due to elevated effective permittivity and absorption; layer thickness variations induce milder effects if total thickness exceeds several penetration depths at 5.8 GHz.

Figure 17 presents the on-body performance of the antenna when positioned 1 mm above the chest, a typical placement for a wearable device. The corresponding return loss (S11) response shows that proximity to the human body introduces loading effects that slightly alter the antenna's performance.

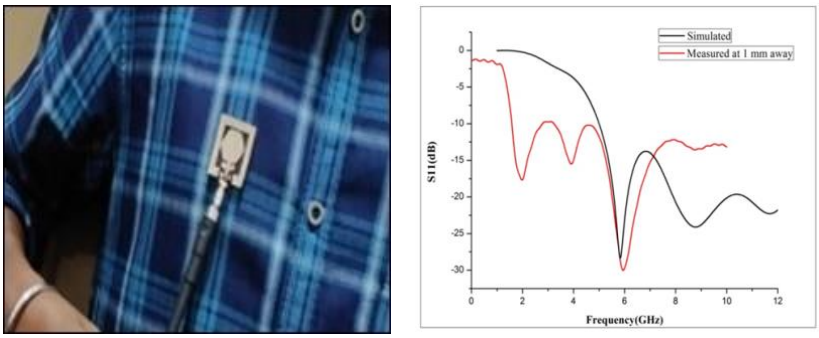

(a) (b)

Fig. 17 .Reflection coefficient (a) On body study (b) S11 vs frequency

While the primary resonance at 5.8 GHz remains well-matched and intact, the coupling between the radiator and the underlying layered tissues of the chest induces slight detuning and creates secondary resonances at adjacent frequencies. This results in a multiband S11 profile, confirming the significant impact of body loading on the antenna's behavior in a realistic use case.

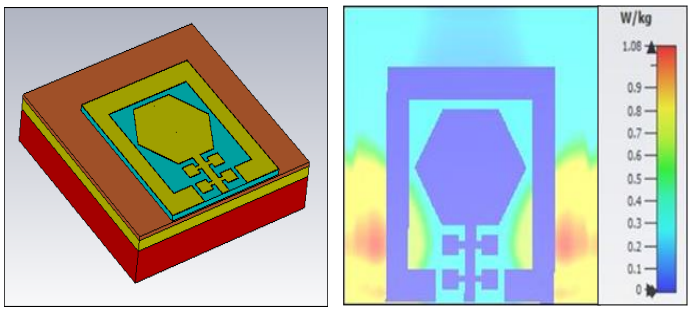

Fig. 18 .SAR Distribution of Antenna at 1 mm gap

Figure 18 shows the simulated Specific Absorption Rate (SAR) distribution for the on-body scenario, assuming a 1 mm standoff from the skin and an input power of 500 mW. The analysis calculates a peak 1-gram averaged SAR value of 1.08 W/kg. This result is well below the 1.6 W/kg safety limit for 1 gram of tissue, as mandated by the IEEE and the U.S. Federal Communications Commission (FCC). The antenna's compliance with this critical safety standard confirms its suitability for use in wearable devices under the specified operating conditions [20].

Table 5 .Comparison of proposed work's antenna specifications to prior works

Ref. no.	Design Dimensions (mm)	Material	Dielectric Constant	Method	S11 (dB)	Gain (dB)	Bandwidth (GHz)	Bending Analysis	SAR (W/Kg)
7	36x30	Cotton	1.7	AMC	<-10	7.2	-	Yes	Yes
8	35.4x82.4	Denim	1.7	EBG	<-10 <-10	7.46 3.62	2.39–2.54 GHz (≈150 MHz).	Yes Yes	Yes Yes
9	40x40	R03003	3	AMC	<-10	-	1.87–3.93 GHz	No	No
11	23.8x34.5	FR4	4.4	partially reflecting surface	<-10	7.02 & 6.12	4.42 & 3.87	No	No
14	32x20	Jean	1.7	CPW with CSRR	-35.42	-6.08	-	No	No

15	80x20	Felt	1.2	CPW with AMC	<-10	2.7	-	No	Yes
16	34x38	Kapton Polyimide	3.4	CPW	<-10	1.822(3.4 GHz) & 1.683(5.7 GHz)	1.64–3.84, 5.52-5.88	Yes	No
17	36x30	Cotton	1.6	CPW with AMC	<-10	7.2	-	No	Yes
27	50x44	Denim	1.7	CPW	<-10	4.67(free space) &- 4.82(on body)	1.15(free space) & 0.9 (on body)	Yes	1.6
28	26x26	FR4	4.3	CPW	<-10	7.3	11	No	No
29	18x18	FR4	4.4	CPW	<-10	2.85 & 4.02	-	No	No
Proposed work	35x30	Felt	1.22	CPW with SIR	-28.33	7.31	3.1 to 10.6	Yes	1.08

All units are in millimeter (mm)

Table 5 provides a technical benchmark of various wearable antennas by comparing their performance across critical electromagnetic and mechanical parameters. The table evaluates antennas fabricated on diverse substrates, including conventional rigid dielectrics like FR4 and R03003 (ε_r = 3.0 to 4.4) and flexible textiles such as cotton, denim, and felt (ε_r = 1.2 to 1.7). The design methodologies vary, with most employing planar structures like coplanar waveguides (CPW), sometimes enhanced with frequency-selective surfaces such as Artificial Magnetic Conductors (AMCs) or Electromagnetic Band-Gap (EBG) structures. The proposed work distinguishes itself by integrating a Stepped Impedance Resonator (SIR) with a CPW feed on a low-permittivity felt substrate (ε_r =1.22). This approach yields a superior balance of performance metrics: a high gain of 7.31 dB, an exceptionally broad -10 dB impedance bandwidth (3.1 to 10.6 GHz), and excellent impedance matching (S11=−28.33dB). Crucially, its performance is validated under bending conditions, and its Specific Absorption Rate (SAR) is confirmed to be within safety limits, demonstrating its robustness and suitability for on-body applications.

4.3. Moisture Measurements

The performance of the textile-based antenna sensor was characterized by first establishing a baseline reference in a fully desiccated state (0% moisture content), where it's initial weight and reflection coefficient (|S11|) were recorded using a precision balance and a calibrated Vector Network Analyzer (VNA). The dry antenna mass is first established from the substrate and conductor contributions; for a 35 × 30 × 2 mm³ felt substrate, the mass is approximately 0.756 g (using 0.36 g/cm³ felt density), and the copper patch mass depends on the patch area A as $m_{Cu} \approx 0.03136A$ g for 0.035 mm copper thickness, giving $m_{dry} \approx 0.756+0.03136A$ g. Distilled water is then added until the antenna reaches $m_{wet}=m_{dry}(1+W)$, where $W=\{0.25,0.50,1.00\}$, and after brief spreading, the $|S11|$ response is recorded; the antenna is dried back to the same mdry between runs to ensure repeatability. Subsequently, moisture content (MC) was incrementally increased by

applying controlled volumes of deionized water to the textile substrate, with the sensor's weight and |S11| response measured at each discrete step after a brief stabilization period. The moisture content for each state was calculated gravimetrically. From Equation 9 key performance metrics, including the resonant frequency (or), minimum |S11| value (return loss), and -10 dB bandwidth, were extracted from the VNA data at each moisture level. The sensor's sensitivity and operational characteristics were then evaluated by analyzing the correlation between the shift in resonant frequency (Δfr) and the corresponding moisture content, thereby generating a calibration curve for moisture sensing [31]. The moisture content in an object expressed in percent $M\ (\%)$ is given as follows:

$$M(\%) = \frac{m_{wet} - m_{dry}}{m_{dry}} x100 \tag{9}$$

Let m_{dry} denote the weight of the object in its completely dry state, and m_{wet} denote the weight after it has absorbed moisture. In Equation (9), the dry weight m_{dry} is employed as the reference; therefore, the moisture content, $M\ (\%)$ is reported on a dry basis. This convention for defining moisture content is applied consistently throughout this study.

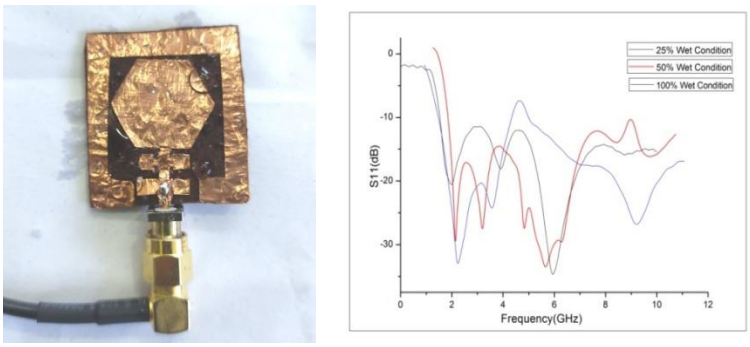

Fig. 19 .Reflection coefficient of proposed design for different moisture contents

Figure 19 presents the |S11| characteristics of the proposed felt-based textile antenna under controlled moisture loading at 25%, 50%, and 100% wetness, defined as the percentage increase in antenna mass over the dry reference. Increasing wetness causes a monotonic downshift of both resonances with slight degradation in return loss minima, attributed to the rise in effective permittivity and loss of the wet substrate. The antenna maintains acceptable performance up to moderate dampness, while full saturation induces severe detuning, particularly in the upper band, confirming moisture as a key performance limiting factor.

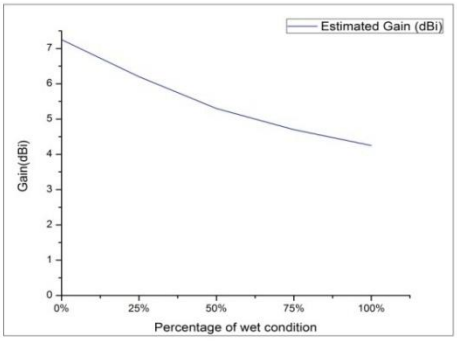

Fig. 20 .Gain analysis with percentage of moisture contents

The plot shown in Figure 20 quantitatively illustrates a critical performance challenge in wearable antenna design: the degradation of antenna gain due to moisture absorption. The graph shows a near-linear decrease in the estimated gain (in dBi) as the percentage of wetness in the antennas substrate increases from 0% to 100%.

4. CONCLUSION

This research presents a compact and flexible hexagonal wideband antenna fabricated on a durable felt substrate for Industrial, Scientific, and Medical (ISM) band applications. The integration of a Stepped Impedance Resonator (SIR) with a Coplanar Waveguide (CPW) feeding structure enables the antenna to achieve high gain while maintaining stable electromagnetic performance under various bending and mechanical stress conditions. The felt substrate's robustness ensures mechanical integrity and consistent operation, crucial for long-term wearable use. The antenna demonstrates excellent on-body compatibility, with Specific Absorption Rate (SAR) values well below established safety limits, ensuring user safety during operation. A distinguishing feature of this design is its dual functionality; it not only facilitates reliable wireless communication but also acts as a sensitive real-time moisture sensor, enabling medical or environmental monitoring via predictable shifts in resonance frequency. Collectively, the results affirm the antenna's viability as a high-performance, multifunctional solution for next-generation wearable devices, seamlessly combining efficient wireless communication with integrated sensing capabilities while providing mechanical durability required for practical wearable applications.

ACKNOWLEDGMENT AND FUNDING

The authors would like to thank GIET University for their valuable guidance and support during the course of this work. This research did not receive any specific grant from funding agencies in the public, commercial, or not-for-profit sectors.

CONFLICT OF INTEREST

The author declared no potential conflicts of interest with respect to the research, authorship, and/or publication of this article.

ETHICS

There are no ethical issues with the publication of this manuscript.

Symbol	Description
C	Equivalent capacitance (F)
E	Electric field strength (V/m)
f, fr, F	Operating / resonant frequency
K	Impedance ratio K=Z2/Z1
L	Equivalent inductance (H)
λ	Wavelength
ℓ_1, ℓ_2	Electrical lengths of narrow and wide SIR sections
R	Equivalent resistance (Ω)

Symbol	Description
S_{11}	Reflection coefficient (return loss)
SAR	Specific Absorption Rate (W/kg)
T	Total electrical length of the resonator
Thickness	Physical thickness of tissue/substrate layers (mm)
VNA	Vector Network Analyzer
VSWR	Voltage Standing Wave Ratio
Z_0	Characteristic impedance of the CPW/microstrip feed line
Z_1, Z_2	Characteristic impedances of high-/low-impedance SIR sections
Zair	Impedance of free space (≈ 377 Ω)
εr	Relative permittivity of substrate
εe	Effective permittivity of transmission line
εr (tissue)	Permittivity of skin, fat, and muscle layers
ρ	Mass density of biological tissue (kg/m³)
ρ (tissue)	Density of specific tissue layers
σ	Electrical conductivity of tissue (S/m)
σ (tissue)	Layer-wise tissue conductivity
tan δ (loss tangent)	Dielectric loss factor of the substrate

REFERENCES

[1] M. A. B. Abbasi, S .Nikolaou, M. A. Antoniades, M. N. Stevanovic, P. Vryonides, "Compact EBG-backed planar monopole for BAN wearable applications", IEEE Transactions on Antennas and Propagation, 2017, vol. 65, no. 2, pp. 453–463.

[2] P. J. Soh, G. A. E. Vandenbosch, S. L. Ooi, N. M. A. Rais, "Design of a broadband all-textile slotted PIFA", IEEE Transactions on Antennas and Propagation, 2012, vol. 60, no. 1, pp. 379–384.

[3] Z. H. Jiang, D. E. Brocker, P. E. Sieber, D. H. Werner, "A compact low-profile metasurface-enabled antenna for wearable medical body-area network devices", IEEE Transactions on Antennas and Propagation, 2014, vol. 62, no. 8, pp. 4021–4030.

[4] A. Valanarasi, R. Dhanasekaran, "Design and analysis of CPW fed flexible CSRR patch antenna for ISM band", Materials Today: Proceedings, 2020, vol. 33, pp. 3026–3030.

[5] F. R. Kareem, M. El Atrash, A. A. Ibrahim, M. A. Abdalla, "All-textile inspired-folded dipole antennas for on/off-body communications medical applications", Alexandria Engineering Journal, 2022, vol. 61, no. 11, pp. 8751–8761.

[6] R.Vashi, T. Upadhyaya, "CPW fed flexible graphene based thin dual band antenna for smart wireless devices", Progress in Electromagnetics Research M, 2020, vol. 89, pp. 73–82.

[7] A. R. Saad, W. M. Hassan, A. A. Ibrahim, "A monopole antenna with cotton fabric material for wearable applications", Scientific Reports, 2023, vol. 13, pp. 1–13.

[8] A. Ejaz, I. Jabeen, Z. U. Khan, A. Alomainy, K. Aljaloud, A. H. Alqahtani, N. Hussain, R. Hussain, Y. Amin, "A high-performance all-textile wearable antenna for wristband application", Micromachines, 2023, vol. 14, pp. 1–15.

[9] A. B. Dey, W. Arif, “On-body low-profile compact AMC-integrated wideband antenna for body area network applications”, IETE Technical Review, 2023, vol. 41, pp. 133–146.

[10] K. N. Ketavath, D. Gopi, S. Sandhya Rani, “In-vitro test of miniaturized CPW-fed implantable conformal patch antenna at ISM band for biomedical applications”, IEEE Access, 2019, vol. 7, pp. 43547–43554.

[11] A. M. Mehta, S. B. Deosarkar, A. B. Nandgaonkar, “Design and development of CPW-fed miniaturized MSA for improved gain, bandwidth and efficiency using PRS”, Progress in Electromagnetics Research C, 2023, vol.137, pp. 211-222.

[12] M. Zhang, M. Li, P. Zhang, K. Duan, B. Jin, L. Huang, Y. Song, “A novel miniaturized bandpass filter basing on stepped-impedance resonator”, Progress in Electromagnetics Research Letters, 2023, vol. 97, pp. 77-85.

[13] U. Rafique, S. U. Din, H. Khalil, “Compact CPW-fed super wideband planar elliptical antenna”, International Journal of Microwave and Wireless Technologies, 2020, vol. 13, pp. 1-8.

[14] S. Ahmad, N. Cherif, S. Naseer, U. Ijaz, Y.S. Faouri, A. Ghaffar, M. Hussein, “A wideband circularly polarized CPW-fed substrate integrated waveguide based antenna array for ISM band applications”, Heliyon, 2022, vol. 8, PP. 1-9.

[15] S. Ahmad, A. Ghaffar, N. Hussain, N. Kim, “Compact dual-band antenna with paired L-shape slots for on- and off-body wireless communication”, Sensors, 2021, vol. 21, pp. 1-16.

[16] A. Ghaffar, W. A. Awan, N. Hussain, S. Ahmad, X. J. Li, “A compact dual-band flexible antenna for applications at 900 and 2450 MHz”, Progress in Electromagnetics Research Lett, 2021, vol. 99, pp. 83-91.

[17] M. A. Shahzad, K. N. Paracha, S. Naseer, S. Ahmad, M. Malik, M. Farhan, A. Ghaffar, M. Hussien, A.B. Sharif, “An artificial magnetic conductor backed compact wearable antenna for smart watch IoT applications”, Electronics, 2021, vol. 10, pp. 1-26.

[18] A. Y. I. Ashyap et al, “Robust and efficient integrated antenna with EBG-DGS enabled wide bandwidth for wearable medical device applications”, IEEE Access, 2020, vol. 8, pp. 56346-56358.

[19] S. Alotaibi, A. A. Alotaibi, “Design of a planar tri-band notch UWB antenna for X-band, WLAN, and WiMAX”, Engineering Technology & Applied Science Research, 2020, vol. 10, pp. 6557-6562.

[20] S. N. Mahmood, A. J. Ishak, T. Saeidi, A. C. Soh, A. Jalal, M.A. Imran, Q. H. Abbasi, “Full ground ultra-wideband wearable textile antenna for breast cancer and wireless body area network applications”, Micromachines, 2021, vol. 12, pp. 1-16.

[21] S. A. Kumar, T. Shanmuganantham, “Design of bending antennas for purpose of biomedical applications using novel approach”, Transaction on Electricals & Electronic Materials, 2021, vol. 22, pp. 725–733.

[22] A. A. Marzah, J. S. Aziz, “Design and analysis of high performance and miniaturized bandpass filter using meander line and Minkowski fractal geometry”, International Conference on New Trends in Computing, Communication, and Information Technology (NTCCIT), 2018, pp. 12–17.

[23] X. Lin, Y. Chen, Z. Gong, B. C. Seet, L. Huang, Y. W. Song, “Ultra-wideband textile antenna for wearable microwave medical imaging applications”, IEEE Transactions on Antennas and Propagation, 2020, vol. 68, pp.4238–4249.

[24] J. Pu, F. Xu, Y. Li, “Miniaturized substrate integrated waveguide bandpass filters based on novel complementary split ring resonators”, International Microwave Biomedical Conference (IMBioC), 2019, pp. 1–3.

[25] S. Kiani, P. Rezaei, M. Fakhr, “A CPW-fed wearable antenna at ISM band for biomedical and WBAN applications”, Wireless Networks, 2021, vol. 27, pp. 735–745.

[26] L. Prasad, B. Ramesh, K. S. R. Kumar, K. P. Vinay, “Design and implementation of multiband microstrip patch antenna for wireless applications”, Advanced Electromagnetics, 2018, vol. 7, pp. 104–107.

[27] D. Gopi, P. V. Kokilagada, S. Gupta, V. R. K. R. Dodd, “Asymmetric coplanar strip-fed textile based wearable antenna for MBAN and ISM band applications”, International Journal of Numerical Modelling, 2021, vol. 34, pp. 1–18.

[28] A. Abdullah Al-Buri, A. Jamal, Zakaria Zahriladha, I. M. Ibrahim, A. Khabba, A. Khaleel Al-Obaidl, T. Aymen Heiyaa Seidi, P. Liton Chandra, "A deep analysis of CPW-fed planar antennas for frequencies 2.6 up to 13.6 GHz", Przegląd Elektrotechniczny, 2023, vol. 99, pp. 155–159.

[29] J. Choi, Y. Oh, J. Choi, K. Y. Jung, "Novel CPW-fed gamma-shaped circularly polarized slot antenna for UWB applications", Journal of Electromagnetic Engineering and Science, 2024, vol. 24, pp. 327–329.

[30] M. Hussain, M. A. Sufian, M. S. Alzaidi, S. I. Naqvi, N. Hussain, D. H. Elkamchouchi, M. F. A. Sree, S. Y. A Fatah, "Bandwidth and gain enhancement of a CPW antenna using frequency selective surface for UWB applications", Micromachines, 2023, vol. 14, pp. 1–13.

[31] D. Bonefacic, J. Bartolic, "Embroidered textile antennas: Influence of moisture in communication and sensor applications", Sensors, 2021, vol. 21, pp. 1–17.

[32] P. Pradeep, M. M. Basha, S. Gundala, J. Syed, "Development of Wearable Textile MIMO Antenna for Sub-6 GHz Band New Radio 5G Applications", Micromachines, 2024, vol. 15, pp. 1-14.

[33] M. A. Abdelghany, M. I. Ahmed, A. A. Ibrahim, A. Desai, M. F. Ahmed, "Textile Antenna with Dual Bands and SAR Measurements for Wearable Communication", Electronics, 2024, vol. 13, pp. 1-19.

[34] N. Nurhayati, D. N. F Agam Nizar, P. Pradini, W. Oce, R. Brian, A. I. Fitri, J. A. Al-Gburi Ahmed, K. V. Atul, J. Safpbri, "Wearable Wideband Textile Coplanar Vivaldi Antenna for Medical and IoT Application", Progress in Electromagnetics Research C, 2024, vol. 148, pp. 145-156.

[35] S. Noghanian, "Textile omnidirectional antenna for wearable WiFi-7 applications using higher order modes", Front. Antennas Propag, 2024, vol. 2, pp. 1-17.

[36] D. Sharma, R. N. Tiwari, D. K. Singh, et al, "A pocket-integrated miniature dual-band and high gain textile MIMO antenna for 5G and WiFi wearable applications", Sci. Rep, 2025, vol. 15, pp. 1-27.

[37] R. K. Baudh, M. Kumar, S. Sahu, M. S. Parihar, D. Kumar V, "A low-profile, wideband, circularly polarized, slotted U-shaped textile antenna for W-BAN applications", ETRI Journal, 2025, vol.47, pp. 579–589.

[38] D. Sharma, R. N. Tiwari, S. Kumar, S. Sharma, L. Matekovits, "A Compact Wearable Textile Antenna for NB-IoT and ISM Band Patient Tracking Applications", Sensors, 2024, vol. 24, pp. 1-18.